



Fermi National Accelerator Laboratory

FERMILAB-Conf-90/86-E
[E-741/CDF]

Large P_t Jets at CDF *

The CDF Collaboration

presented by

Mauro Dell'Orso
*Universita' di Pisa
Pisa, Italy*

May 9, 1990

* To be published in the proceedings of the Les Rencontres de Physique de la Vallee D'Aosta, La Thuile, Italy, March 18-24, 1990.



LARGE P_t JETS AT CDF

CDF Collaboration*
Presented by Mauro Dell'Orso

Dipartimento di Fisica, Università di Pisa
Pisa, ITALY

ABSTRACT

The inclusive jet cross section and the dijet mass spectrum have been measured at the Fermilab Tevatron Collider at $\sqrt{s} = 1.8$ TeV. These measurements span approximately 7 orders of magnitude in cross section and contain jets up to 400 GeV in transverse energy and dijet masses up to 950 GeV. Comparisons have been made to QCD at both orders α_s^2 and α_s^3 .

* The collaborating institutions are listed in Appendix

1 Introduction

In the 1988-1989 CDF run at the Fermilab Tevatron Collider, approximately 4.5 pb^{-1} of data were collected at $\sqrt{s} = 1.8 \text{ TeV}$. The jets in this sample range from 30 GeV to over 400 GeV in transverse energy and span 7 order of magnitude in cross section. Presented in this paper are a measurement of the inclusive jet cross section, and a measurement of the dijet invariant mass (M_{jj}) spectrum.

The interest for such measurements at the highest jet energies is manifold.

- a) Comparisons to QCD can be made over a large range of E_t and the point-like scattering of partons can be probed at distances smaller than $5 \times 10^{-17} \text{ cm}$ [1].
- b) The variation of cross section with the jet cluster cone size, featured by the α_s^3 QCD predictions now available [2], can be studied.
- c) New and unexpected physics can show up as resonance bumps in the mass spectrum or, for negative results, limits can be defined on the mass of new particles.
- d) A detailed study of the dependence of the mass spectrum on the number of jets helps in the difficult issue of analyzing the characteristics of gluon radiation in the scattering process.

2 Data Selection

The CDF detector has been described in detail elsewhere [3]. For these measurements jets in the central scintillator calorimeters were used. The event vertex was required to be within 60 cm from the center of the detector to keep the events inside the geometrical acceptance. The data were collected using single jet online triggers, which basically required the presence of at least one energy cluster in the calorimeter with a transverse energy greater than, respectively, 20, 40, and 60 GeV. The 20 and 40 GeV triggers were pre-scaled.

Offline jets are clustered with a fixed cone size algorithm [4]. The cone size is defined by $R = (\Delta\eta^2 + \Delta\phi^2)^{1/2}$, where η and ϕ represent the pseudorapidity and azimuthal angle. The algorithm also gives the momentum of each jet, assuming a massless particle for each calorimeter tower belonging to the cluster.

Cosmic rays, which can deposit significant amounts of energy by bremsstrahlung, were removed using timing information in the hadron calorimeter. The remaining background events were rejected on the basis of: the average electromagnetic fraction, the average charge/total energy, the missing E_t significance. The estimated contamination after these cuts is less than 1% for jets with $E_t > 150 \text{ GeV}$ [5].

3 Detector Response

The effects of resolution smearing and energy degradation due to calorimeter non-linearities, uninstrumented regions of detector, etc. can distort the measured spectra. In order to take into account these effects, a Montecarlo was used. It was tuned to reproduce

the calorimeter response to single pions observed in the test beam and the jet fragmentation observed in the data. The E_t and the M_{jj} response functions were then extracted. These informations were used when comparing the data to the theoretical predictions.

Since only higher order QCD calculations can reproduce the dependence of the measurement on the cone size [2], an out-of-cone correction has been applied to the jet energies when measuring the M_{jj} spectrum, for which only leading order predictions are available. The average energy lost out of the cone has been studied as a function of the jet energy. Fig. 1 shows the average energy flux around the jet axis as a function of $\Delta\phi$ for clean two-jet events. The energy level at 90° from the jets has been ascribed to the underlying event and not considered belonging to the hard scattering. The energy outside the clustering cone, and in excess of the underlying event level, is defined as energy lost out of the cone and its measurement used to estimate the out-of-cone correction. The effect of these losses on the cross section is evident in fig. 2 which shows the ratio of the M_{jj} spectrum with out-of-cone correction to the spectrum without correction.

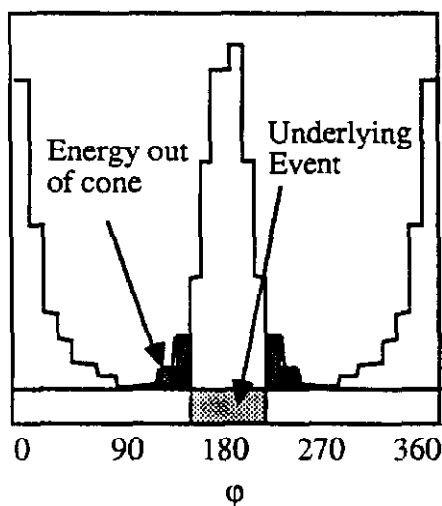


Fig. 1: Average Jet Profile

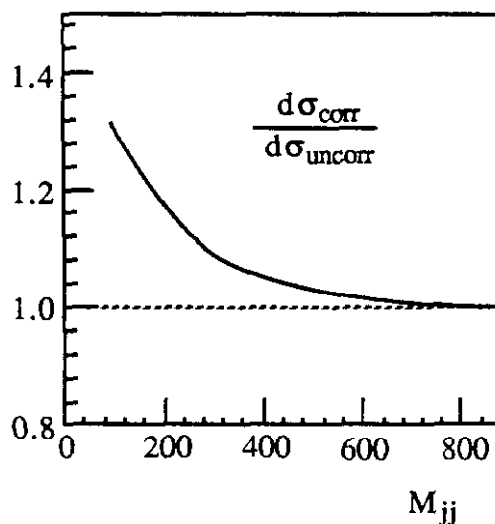


Fig. 2: Effect of Out-of-Cone Correction

4 Systematic Uncertainties

The major sources of systematic error on the jet energy scale result from uncertainty on the calorimeter response, on the fragmentation tuning, and on the energy from the underlying event.

The dominant uncertainty in the detector response for jets containing low energy pions (less than 25 GeV) comes from the uncertainty on the low energy response. For jets containing pions with energies greater than 25 GeV, the dominant uncertainty comes from the modeling of the response in the azimuthal boundary regions between calorimetry cells.

The uncertainty on the fragmentation tuning is correlated with the track efficiency, since

the fragmentation was measured from the data. The tracking efficiency for tracks in the jet core was varied in the simulation within its uncertainty of 7%, to give the corresponding uncertainty on the energy scale.

Due to differences in the definition of the underlying event, there is a 540 MeV uncertainty in the underlying event, for a cone radius of 0.7.

Adding all these uncertainties in quadrature, the overall systematic error on the jet energy scale varies from 4% at 20 GeV to 3% at 400 GeV. A conservative 8% uncertainty was assigned to the jet energy resolution, comparing the results of E_T balancing studies in two-jet events for data and simulation. Finally, a 15% systematic uncertainty was assigned to the measurement of the integrated luminosity. The average overall systematic error on the cross section is of the order of 35%.

5 Inclusive Jet Cross Section

For this measurement jets in the central pseudorapidity region ($0.1 < |\eta| < 0.7$) were selected. Fig. 3 shows the differential jet cross section as a function of E_T for a cone size of 0.7 compared to a leading order QCD calculation. The data were corrected using the detector response, the underlying event energy was subtracted, and no out-of-cone correction was applied. The QCD prediction was normalized to the data by minimizing the χ^2 in a limited range of E_T . QCD and compositeness will agree in shape in some E_T range and disagree at high E_T . Therefore, in order to search for compositeness, the predictions are normalized in the region where they agree and the data are compared to the predictions in the high E_T region.

A slight excess of events in the high E_T region can be seen in fig. 3. The statistical level of this excess, however, is only 2.5 to 3.5 standard deviations and it will be reduced some more when the systematic error will be taken into account. The reason for not using yet the systematic error is that bin to bin correlations of the systematic uncertainties are still under study.

Fig. 4 shows the same data now compared to next-to-leading order QCD, where the QCD normalization is absolute. The comparison on absolute scale is interesting here, since the next-to-leading order prediction has a reduced theoretical uncertainty.

A comparison is also made to next-to-leading order QCD in fig. 5. The top plot in this figure shows the cross section as a function of cone size for 100 GeV E_T jets. The data appear to be consistent with QCD within the systematic uncertainty on the vertical scale. To get rid of most of the systematic uncertainty and compare the slope of the data to the slope of the prediction, the bottom plot in fig. 5 shows the ratio of the cross sections to the cross section for jets with cone size of 0.7. In this plot the data appear to have a steeper dependence on the cone size than what α_s^3 calculations would predict.

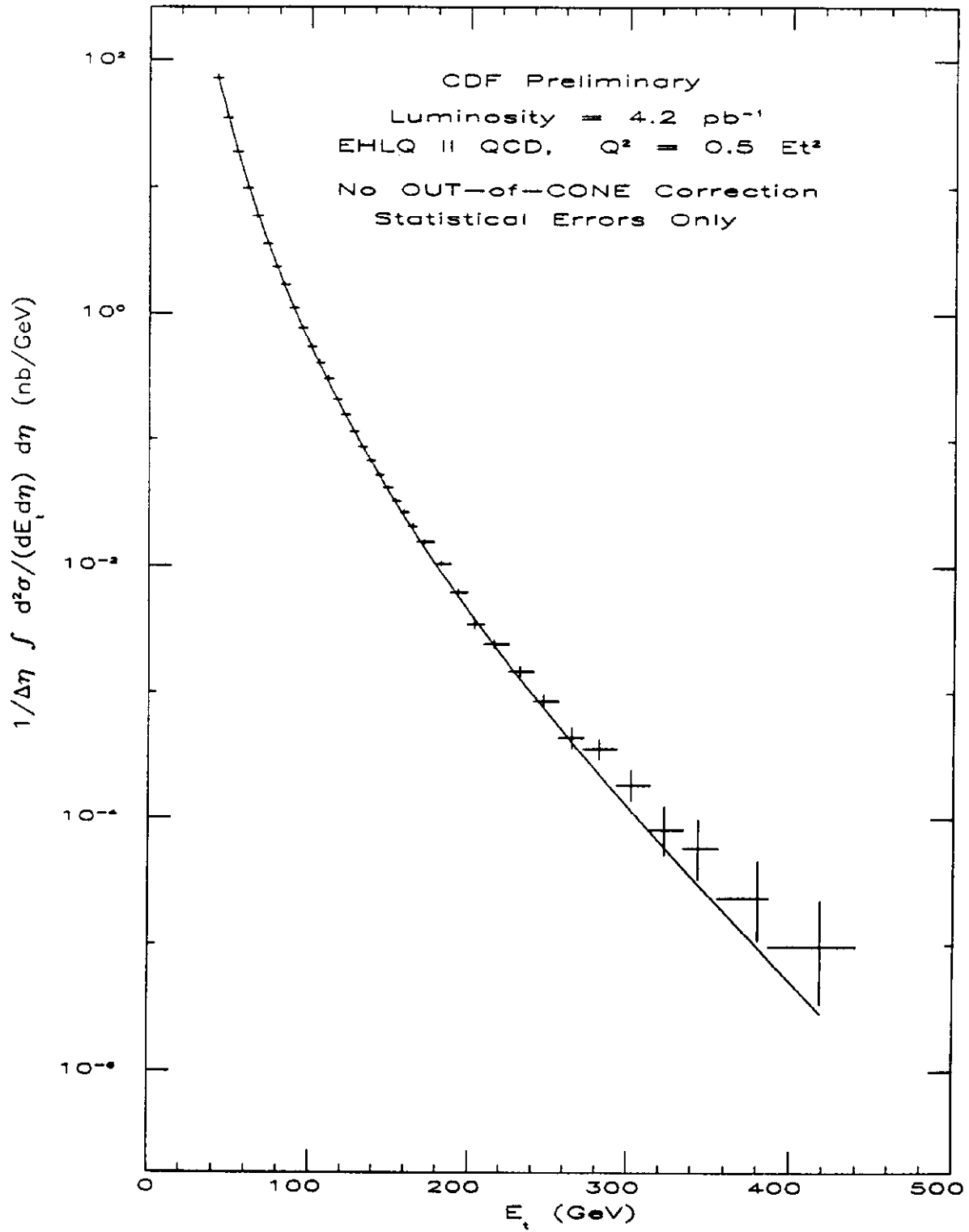


Fig. 3: Inclusive Jet Cross Section compared to leading order QCD

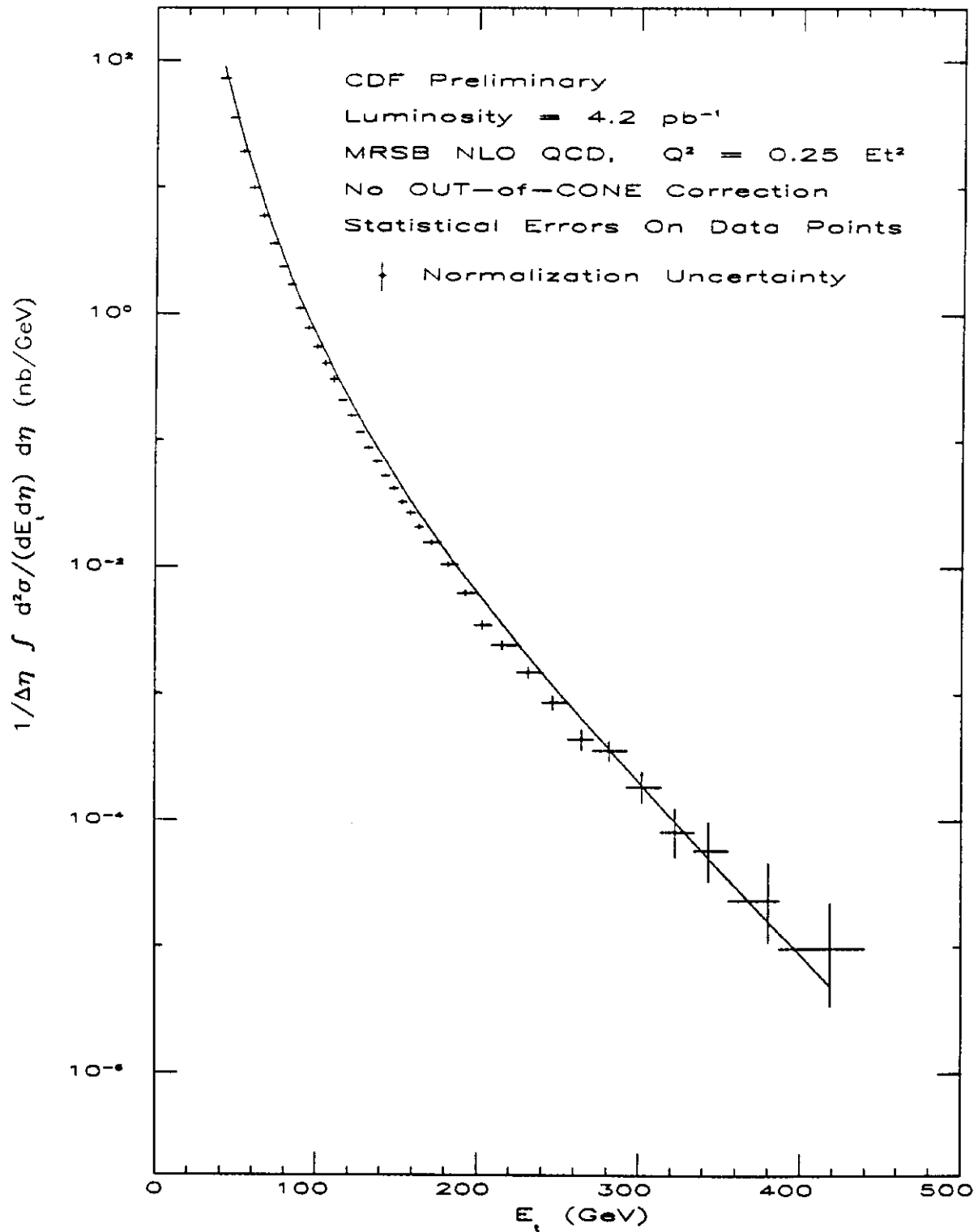


Fig. 4: Inclusive Jet Cross Section compared to next to leading order QCD

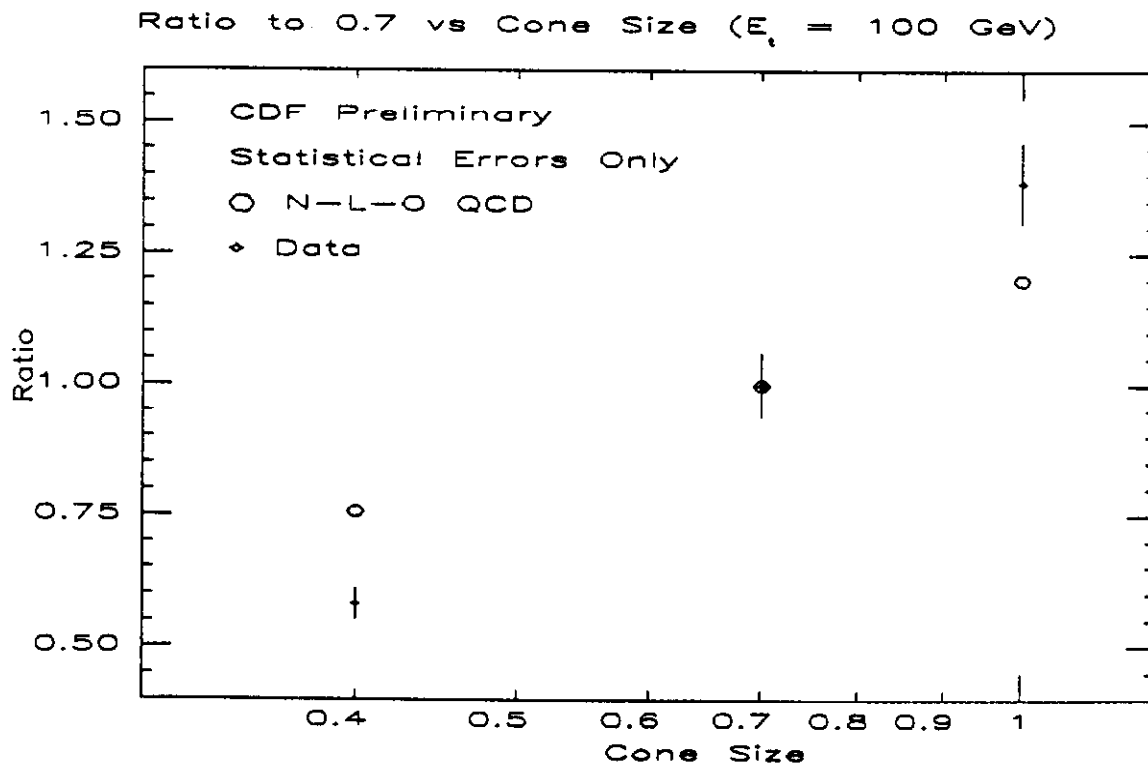
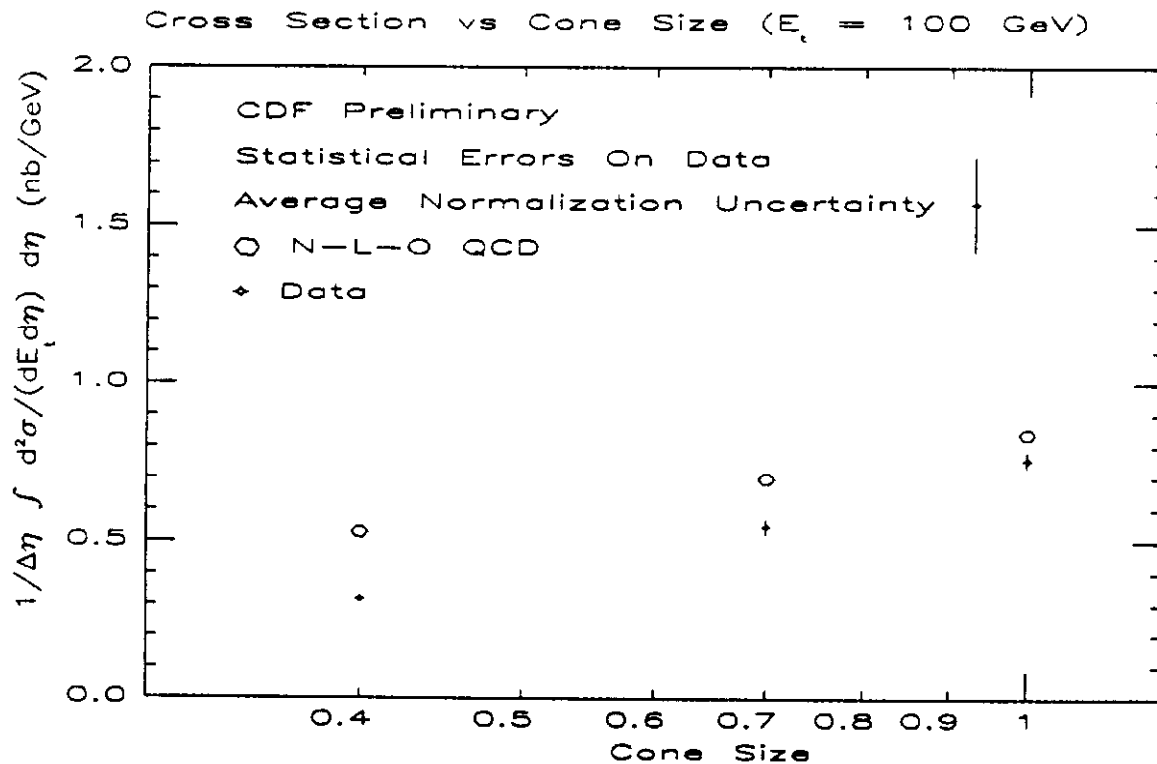


Fig. 5: Cross Section as a function of Cone Size

6 Dijet Mass Spectrum

For this measurement the two leading jets were required to be in the central pseudorapidity region ($|\eta| < 0.7$). An additional cut was applied, requiring the two leading jets to be back to back within 30° in the azimuthal plane. This is a loose cut to reject multijet events. The underlying event subtraction and the out of cone correction were applied. The dijet invariant mass was calculated as $M_{jj} = [(E_1 + E_2)^2 - (\mathbf{P}_1 + \mathbf{P}_2)^2]^{1/2}$, where E_i and \mathbf{P}_i are the measured energies and momenta of the two leading jets. Instead of correcting the data for the finite resolution, the theoretical predictions were smeared using the M_{jj} detector response [6]. This procedure simplifies the search for bumps, since correcting the data would require in input the data line shape.

Fig. 6 shows the plot of the measured differential cross section $d\sigma/dM_{jj}$ as a function of the dijet invariant mass M_{jj} . The dots represent the experimental points with their statistical errors. The two dashed lines in fig. 6 define a band of uncertainty in the theoretical prediction. To obtain this band we calculated the predictions for the leading order QCD diagrams, varying the Q^2 in the range $0.5P_t^2 < Q^2 < 2P_t^2$ and using different parametrizations for the structure functions, namely EHLQ1, EHLQ2, DO1, DO2 [1,7]. The band in fig. 6 is the envelope of all the predictions for different Q^2 s and structure functions. It should be noted that these QCD predictions refer to the leading order QCD matrix element and do not take into account gluon radiation from the initial and final state partons.

Since both data and theory have a normalization uncertainty, we normalized the theoretical predictions on the data to have a more quantitative test of QCD. Only the statistical error was used in the fits. The systematic error is still to be included in the fits before getting a final conclusion, but it is already possible to observe that the M_{jj} spectrum is sensitive to differences between structure functions. The structure function DO2 with $Q^2 = 0.5P_t^2$ shows the best agreement with the data in terms of χ^2 . The solid line of fig. 6 shows this prediction.

The worse agreement with the data is given by the structure function EHLQ2. The difference between the two fits is shown on linear scales in fig. 7, where the quantity $(\text{Data} - \text{QCD}) / \text{QCD}$ is plotted for the two predictions. The dashed lines represent the same theoretical band of fig. 6 and the first bar on the left side shows the size of the average systematic error.

To illustrate the sensitivity of the mass spectrum to the quark compositeness, we fitted on the data the predictions obtained adding an effective 4-quark contact interaction [1] to the standard QCD lagrangian. Fig. 8a shows the predictions for different values of the compositeness energy scale Λ^* ; as $\Lambda^* \rightarrow \infty$ the predictions approach the pure QCD calculation. The curves are calculated at $Q^2 = P_t^2$ using the structure function DO2. Fig. 8b,c,d show the same predictions on linear scales. These data confirm the present CDF

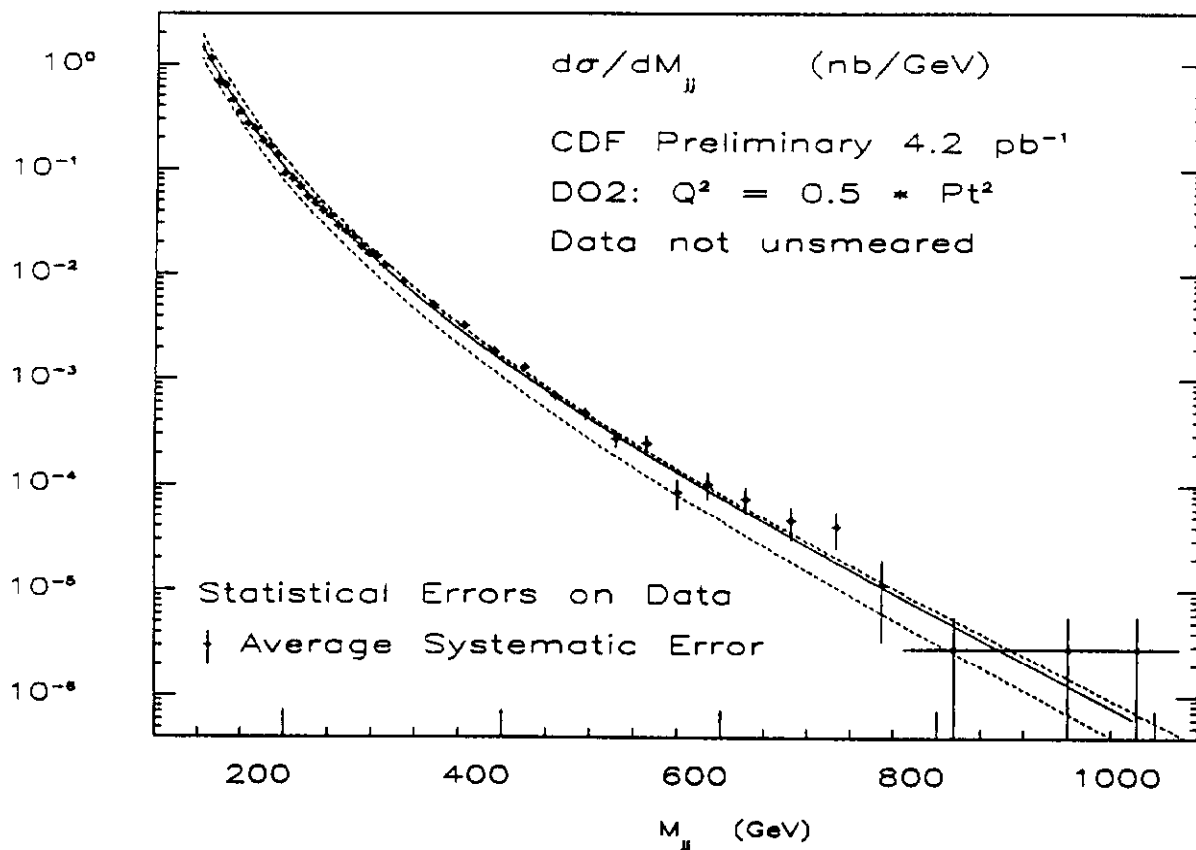


Fig. 6: Dijet Mass Spectrum

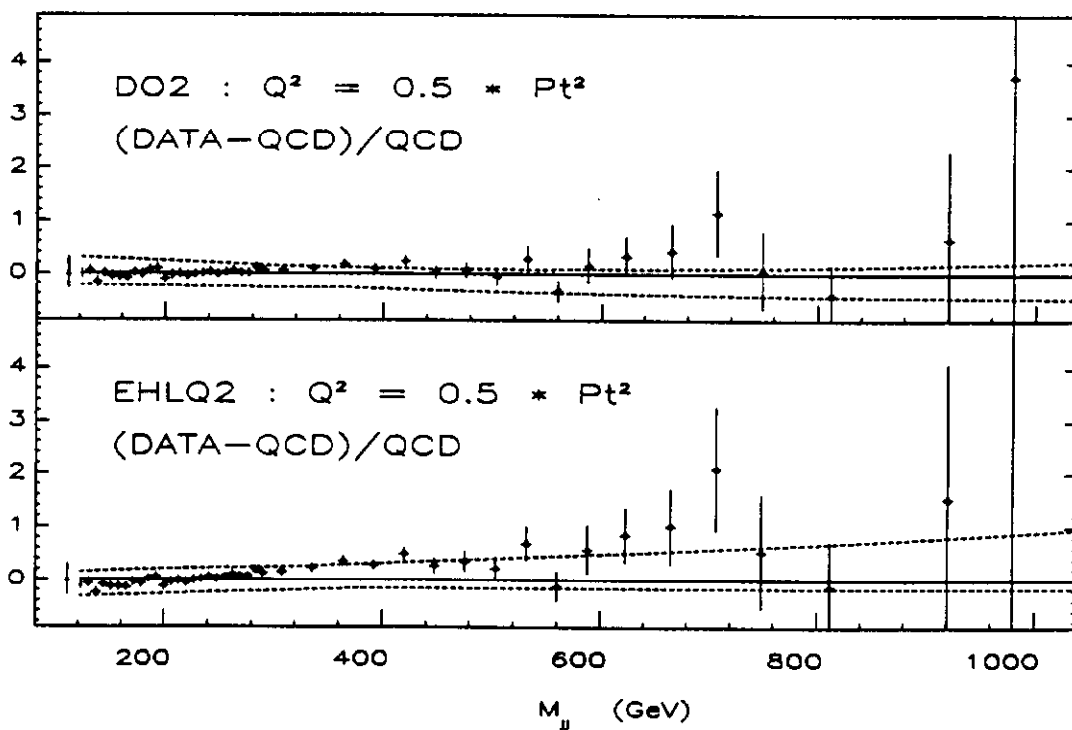


Fig. 7: Predictions from different Structure Functions

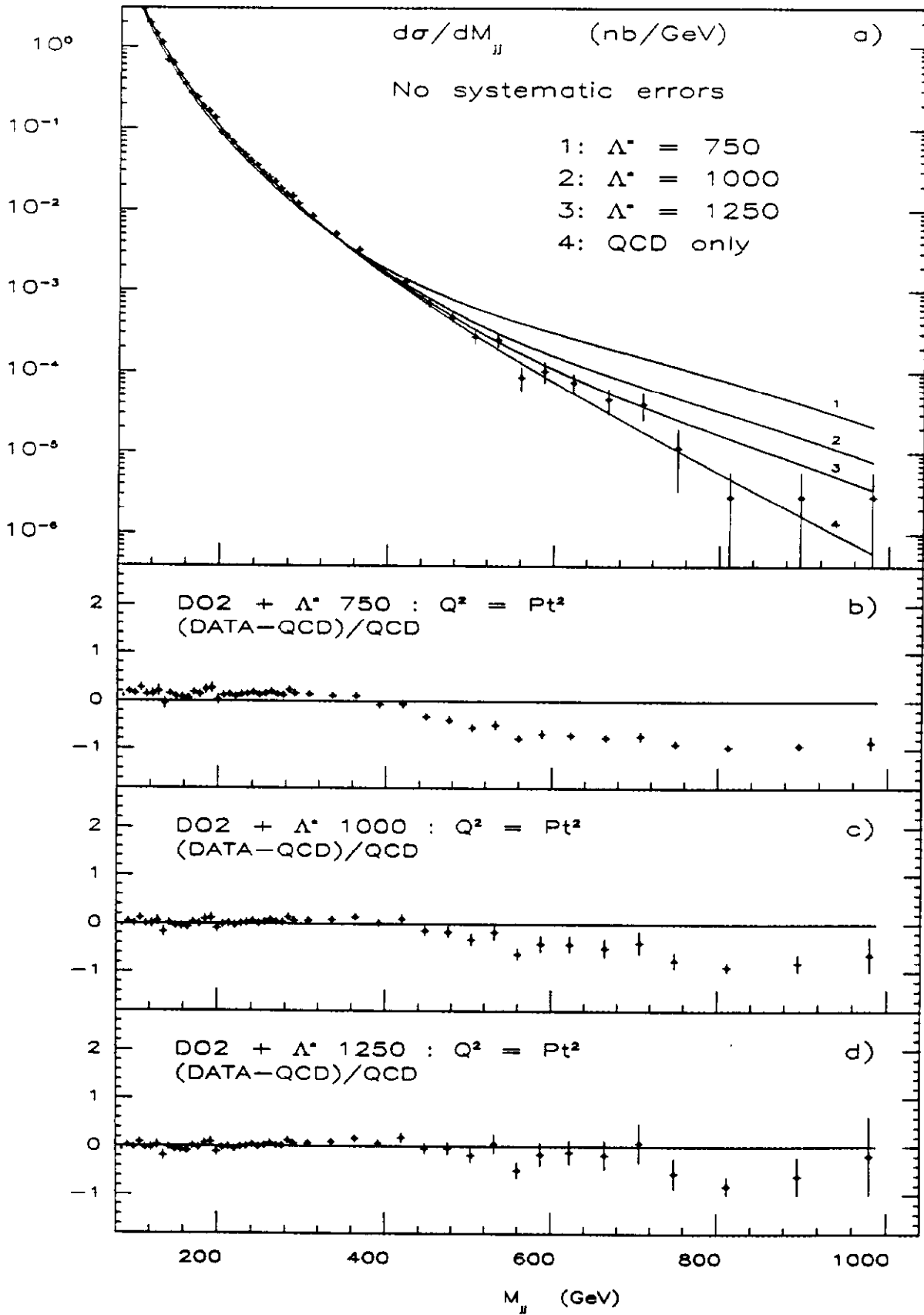


FIG. 8: Predictions with Different Compositeness Scales

limit of $\Lambda^* > 950$ GeV, but the systematic error is to be included in the fit before giving the new limit.

7 QCD Radiation

As we said, a direct comparison of the measured mass spectrum with the $2 \rightarrow 2$ QCD calculation does not include the possibility of gluon radiation which generates secondary jets.

To measure the effect of the radiation on the cross section we added the non-leading jets in the computation of the invariant mass, whenever the distance (in η - ϕ space) from one of the leading jets was smaller than a fixed radius R_{cut} . The cut is intended to reject the jets generated by initial state radiation, which are likely to be away from the directions of the final state partons. We then looked at the dependence of the mass spectrum on the value of R_{cut} .

Fig. 9 shows how the cross section changes as R_{cut} changes. This figure shows, for different values of the sum cone radius R_{cut} , the ratio of the mass spectrum with the jet merging to the mass spectrum of the two leading jets. The effect grows up to a factor 1.7 for a radius $R_{\text{cut}} = 1.5$. The ratio is roughly constant as a function of the mass. This means that the radiation affects the absolute scale of the cross section more than the shape of the distribution.

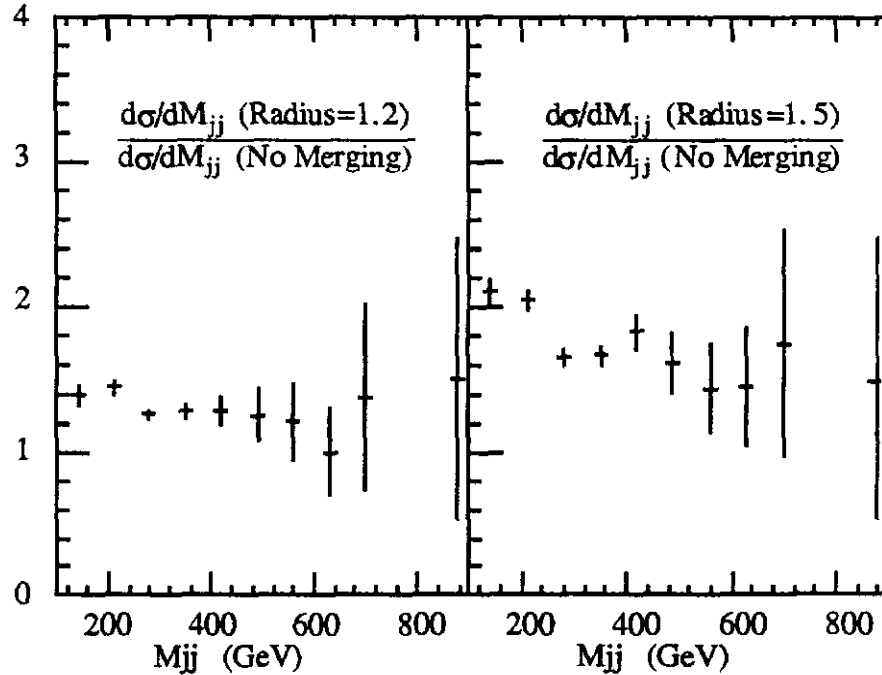


Fig. 9: Effect of the Jet Merging Procedure

8 Summary

a) We measured the inclusive differential jet cross section $d\sigma/dE_t$ at $\sqrt{s} = 1.8$ TeV and in the

E_T range from 30 to 400 GeV. Investigations of the dependence of jet cross section with cone size have begun.

- b) We measured the differential dijet cross section $d\sigma/dM_{jj}$ in the dijet invariant mass (M_{jj}) range from 100 to 950 GeV.
- c) The data appear to be consistent with both leading and next to leading order QCD predictions. The spectra are sensitive to differences between structure functions and other parametrizations for the structure functions are under test. A small excess of events is observed at high E_T , over the leading order QCD prediction. Correlations in the systematic uncertainties are under study, however the previous CDF limit of 950 GeV for the quark compositeness scale Λ^* is still valid.
- d) The mass spectrum is less inclusive than the E_T spectrum and it is more sensitive to the details of the QCD radiation, allowing probing of theoretical predictions.
- e) We have in progress detailed tests on possible structures in the mass spectrum to give limits on the axigluon [8] mass and to search for bumps, using cuts that enhance the resolution.

9 Appendix

Collaborating institutions:

Argonne National Laboratory - Brandeis University - University of Chicago - Fermi National Accelerator Laboratory - Laboratori Nazionali di Frascati of the Istituto Nazionale di Fisica Nucleare - Harvard University - University of Illinois - National Laboratory for High Energy Physics (KEK) - Lawrence Berkeley Laboratory - University of Pennsylvania - Istituto Nazionale di Fisica Nucleare, University and Scuola Normale Superiore of Pisa - Purdue University - Rockefeller University - Rutgers University - Texas A&M University - University of Tsukuba - University of Wisconsin

References

- [1] E. Eichten et al., *Rev. Mod. Phys.* **56** (1984) 579.
- [2] S.D. Ellis et al., ETH-TH/90-3 (1990); F. Aversa et al., LNF-90/012 PT (1990).
- [3] CDF Collaboration, *Nucl. Instr. and Meth.* **A267** (1988) 249, 257, 272, 280, 301, 315, 330; **A268** (1988) 24, 33, 41, 46, 50, 75, 92.
- [4] D. Brown et al., CDF Internal Note **605** (1988).
- [5] T. Hessing, CDF Internal Note **957** (1989).
- [6] M. Dell'Orso et al., CDF Internal Note **1056** (1989).
- [7] D. Duke and J. Owens, *Phys. Rev.* **D30** (1984) 49.
- [8] P.H. Frampton and S.L. Glashow, *Phys. Lett.* **B190** (1987) 157.